

# Mode-selective photoisomerization in 5-hydroxytropolone. I. Experiment

Frederick A. Ensminger, Jason Plassard, and Timothy S. Zwier<sup>a)</sup>  
Department of Chemistry, Purdue University, West Lafayette, Indiana 47907-1393

Steven Hardinger  
Department of Chemistry, California State University, Fullerton, California 92634

(Received 7 October 1994; accepted 20 December 1994)

Laser-induced fluorescence excitation, dispersed fluorescence, and population labeling spectra of the  $S_0-S_1$  transition of 5-hydroxytropolone (5-HOTrOH) have been recorded in a supersonic free jet. In the ground state, the two in-plane orientations of the 5-OH substituent produce two isomers, *syn* and *anti* relative to the 2-OH. Population labeling is used to identify transitions in the spectrum originating from the *syn* and *anti* zero-point levels. In the excited electronic state where 2-OH H-atom tunneling is expected to be more facile, the single vibronic level dispersed fluorescence spectra identify excited state levels with widely varying *syn-anti* character. Many of the levels in the low-energy region of the spectrum are nearly pure *syn* or *anti* in character, thereby showing little coupling to the isomerization reaction coordinate. Other levels are strongly *syn-anti* mixed via Fermi resonance interactions. A few levels exhibit strong *syn-anti* mixing despite being relatively isolated from other levels. These levels have strong *syn-anti* coupling matrix elements which reflect a strong coupling to the reaction coordinate. Analysis of the dispersed emission identifies a "promoter" vibrational mode W, with *syn* (*anti*) ground-state frequency 336 (337)  $\text{cm}^{-1}$  which appears to play a key role in coupling *syn* and *anti* levels. The accessibility of excited state levels of mixed character makes it possible to efficiently and reversibly isomerize 5-hydroxytropolone in a highly mode-specific fashion. © 1995 American Institute of Physics.

## I. INTRODUCTION

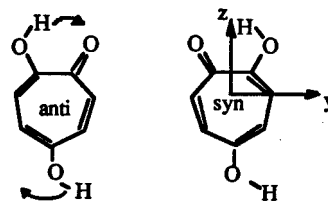
In the pursuit of vibrationally mode-selective reactivity, molecules undergoing intramolecular photoisomerization have drawn considerable attention.<sup>1-3</sup> Part of the allure of such studies is that reaction occurs between well-defined reactant and product geometries, often with a simple spatial coordinate as the reaction coordinate. The desired ideal is that certain normal coordinates will be more strongly coupled to the reaction coordinate than others. Excitation of these coordinates then could lead to enhanced reactivity. Of course, as in bimolecular<sup>4,5</sup> and photodissociation<sup>6</sup> reactions, mode-selective photoisomerization is possible only if reaction occurs at low enough state densities that intramolecular vibrational redistribution is unimportant on the time scale of reaction.

Isomerization reactions driven by hydrogen-atom or proton tunneling are especially intriguing candidates for mode selectivity because reaction can occur at energies well below the classical transition state. In addition, tunneling is especially sensitive to the positions of the heavy atoms serving as donor and acceptor, raising the prospect of vibrationally mode-selective behavior.

This paper presents a single vibronic level study which shows strong vibronic state selectivity in the photoisomerization of 5-hydroxytropolone (5-HOTrOH). Our work builds on previous studies of tropolone,<sup>7-10</sup> a pseudoaromatic molecule containing a seven-membered ring which can undergo hydrogen atom tunneling between the oxygen atoms in a symmetric double-minimum potential well. In tropolone, spectacular mode-specific changes in the H-atom tunneling

splitting have been observed,<sup>7-10</sup> demonstrating the exquisite sensitivity of H-atom tunneling to the heavy atom motion in the rest of the molecule. As we will see, the mode specificity in the isomerization of 5-hydroxytropolone is made possible by this same H-atom tunneling reaction coordinate and its sensitivity to vibration.

In 5-HOTrOH (shown below), despite the symmetric position of hydroxy substitution, the preference of the 5-OH hydroxy group for in-plane positions<sup>11,12</sup> produces a slight asymmetry in the molecular potential energy surface. Based on our recent work on 5-aminotropolone,<sup>13</sup> where the asymmetry of the NHD isotope was sufficient to quench H-atom tunneling in the ground state, one might expect a similar quenching in 5-HOTrOH. Two distinct conformers are then formed which differ in the orientation of the 5-OH hydrogen relative to the tunneling hydrogen. "Syn" ("*anti*") designates that the 5-OH and 2-OH are on the same (opposite) side of the  $z$  inertial axis indicated below. In 5-HOTrOH there are two well-defined reaction coordinates for the *syn-anti* isomerization involving (i) H-atom tunneling between the two oxygen atoms and (ii) 5-OH torsion through 180 degrees.



In a recent communication,<sup>14</sup> we reported initial results of our study of 5-HOTrOH which focused attention primarily on the  $S_0-S_1$  electronic origins for the two isomers. Figure

<sup>a)</sup> Author to whom correspondence should be addressed.

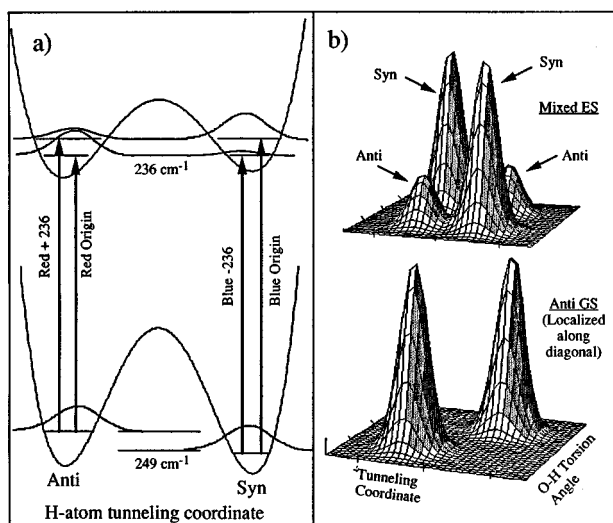


FIG. 1. (a) Potential energy curves along the intramolecular H-atom tunneling coordinate. Note the reversal in stability between  $S_0$  and  $S_1$ . The  $S_0$  energy difference of  $249\text{ cm}^{-1}$  and the  $S_1$  energy difference of  $236\text{ cm}^{-1}$  account for the  $485\text{ cm}^{-1}$  difference between the red and blue origins. Localized ground-state wave functions and partially delocalized excited state wave functions provide nonzero Franck–Condon intensity in the red+236 and blue–236 “crossover” origin transitions. (b) 2D wave functions for *anti*  $0_0$  and the nominally *syn*/blue  $0_0$  levels associated with the red+236 crossover origin transition. Since the *syn*  $0_0$  wave function (not shown) is localized along the opposite diagonal, the emission spectrum is predominantly to *syn* ground-state levels.

1(a) presents a schematic diagram of these transitions and of the “crossover” transitions which promote *syn*↔*anti* isomerization in the molecule. We argued previously that the presence of the crossover transitions signals that the excited state levels have mixed *syn*–*anti* character, as shown in the two-dimensional wave functions of Fig. 1(b). As we will see, such mixed-character excited vibronic states are more the rule than the exception, presenting a delightful venue for the study of mode specificity in intramolecular photoisomerization.

The 5-OH substitution has a similar effect<sup>1</sup> to the asymmetric methyl<sup>15,16</sup> and phenyl<sup>17</sup> substitutions on 9-hydroxyphenalenone, whose spectroscopy has been studied in some detail in a matrix. The isomerization of 5-HOTrOH also bears some resemblance to the keto-enol isomerization of “double” benzoxazole studied recently by Ernsting *et al.*<sup>18</sup> By comparison to this work, a pleasing feature of 5-HOTrOH is its small ground-state asymmetry which enables the study of the isomerization on a state-to-state basis following excitation out of either ground-state well.

In the present paper, we present a complete account of our work on 5-HOTrOH which extends the previously reported results<sup>14</sup> in several ways. First, the primary focus of this paper shifts from the *syn* and *anti* origins to vibronic levels above the origin. Second, dispersed emission scans are used to quantify, to the extent possible, the fractional *syn* and *anti* characters of each of the major levels in this region. Third, in a few cases, we have identified the vibrational state character of the *syn* and *anti* levels involved in the mixing.

These identifications have led to a classification of the types of mixing present. Furthermore, the analysis identifies a promoter mode whose excitation, more than any other mode, enhances *syn*–*anti* mixing. Finally, in the adjoining paper, we present *ab initio* calculations in which several aspects of the multidimensional reaction surface are explored. A normal coordinate analysis shows two possible in-plane modes which correlate well with the observed promoter mode.

## II. EXPERIMENT

Laser-induced fluorescence (LIF) excitation and dispersed fluorescence spectra were recorded using an apparatus which has been described previously.<sup>19</sup> A solid sample of 5-hydroxytropolone was resistively heated to  $115\text{--}120\text{ }^\circ\text{C}$  in a housing placed directly before a pulsed nozzle (General Valve,  $500\text{ }\mu\text{m}$  diameter). Helium gas at a pressure of 2–10 bar was passed over the heated sample and expanded through the nozzle into a chamber pumped by two vapor booster pumps operating in parallel. The output of an excimer-pumped dye laser (Lambda-Physik EMG-50E/FL2001, PBBO or BBQ dye) crossed the expansion 1–2 cm downstream from the nozzle. Unsaturated excitation spectra require unfocused laser energies of about  $10\text{ }\mu\text{J/pulse}$ . Dispersed fluorescence spectra utilize a  $3/4\text{ m}$  monochromator operating at a resolution of  $10\text{ cm}^{-1}$  FWHM. Fluorescence signals were detected by a UV-sensitive photomultiplier tube using gated integration (Stanford Research SR250). A cut-off filter was used in the fluorescence excitation scans to reduce scattered laser light.

In 5-hydroxytropolone, two ground-state levels (the *syn* and *anti* zero-point levels) possess sufficient population to contribute to the excitation spectra. In order to identify transitions out of a specific ground-state level, population labeling scans were recorded. Fluorescence-difference spectra are recorded by measuring the difference between a normal excitation spectrum and one in which the population in a given ground-state level is depleted. The difference between the normal and depleted spectra yields only transitions from the targeted level.

In practice, population is removed by a saturating laser pulse operating at half the repetition rate of the probe laser. The saturation laser (operating at 20 Hz) is set on a transition out of a targeted ground-state level, while the probe laser (operating at 40 Hz and delayed by 100 ns from the saturation laser) is tuned through the desired region of the spectrum. Fluorescence signal from the probe laser with and without the saturation laser present alternates between that due to the depleted and normal spectra, respectively. Subtraction was performed on a shot-to-shot basis by using the active base line subtraction mode of the gated integrator.

5-HOTrOH was synthesized at Cal State Fullerton using the procedure of Russell *et al.*<sup>20</sup>

## III. RESULTS AND ANALYSIS

### A. Fluorescence excitation and population labeling spectra

Figure 2 shows an overview fluorescence excitation scan of the first  $1600\text{ cm}^{-1}$  of the  $S_1\leftarrow S_0$  transition of

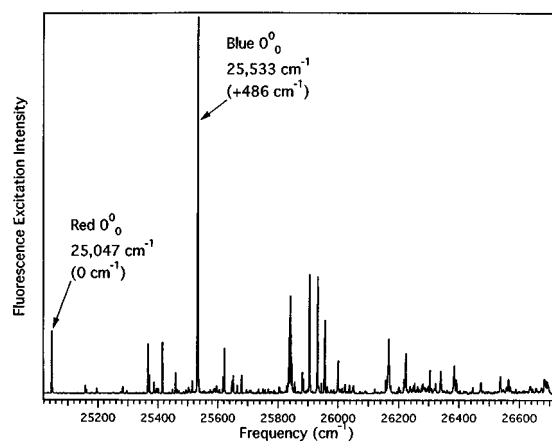


FIG. 2. Overview fluorescence excitation scan of the first  $1600\text{ cm}^{-1}$  of the  $S_1 \leftarrow S_0$  transition of 5-hydroxytropolone. Two origins due to *anti* (“Red”  $0_0^0$ ) and *syn* (“Blue”  $0_0^0$ ) conformational isomers are marked in the figure.

5-HOTrOH. The scan was taken under unsaturated conditions and is power-normalized. As dispersed fluorescence and population labeling spectra will show, the two transitions marked in the figure are  $S_1 \leftarrow S_0$  origins due to the two conformational isomers, *anti* and *syn*. Arguments will be presented shortly that the “red” origin at  $25\,047\text{ cm}^{-1}$  is most likely due to the *anti* ground-state isomer while the “blue” origin ( $25\,533\text{ cm}^{-1}$ ) originates from the *syn* ground state. Throughout the rest of the paper we will assume this isomeric assignment.

In assigning transitions above the origin, several difficulties are encountered. First, the spectra due to the two isomers are similar, but far from identical. Second, correlations to levels in the spectra of tropolone<sup>7–10</sup> and aminotropolone<sup>13</sup> are not easily made, though gross similarities exist. Third, the interleaved spectra from the two isomers makes it difficult to assign a given feature to a given isomer.

As an aid to the assignment process, population labeling spectra have been recorded with the saturation laser tuned to the blue and red origins. Figure 3 compares the fluorescence

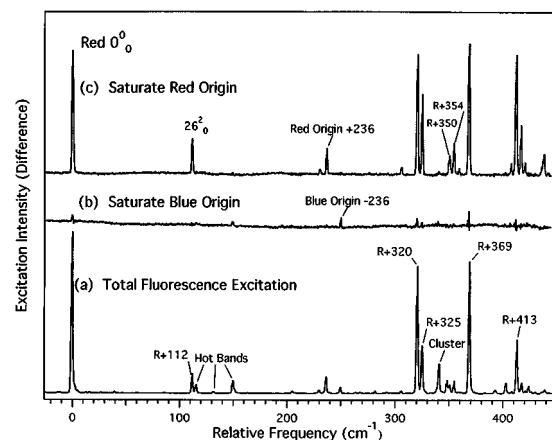


FIG. 3. (a) Fluorescence excitation spectra of the region near the red origin in 5-hydroxytropolone. (a) Total fluorescence, (b), (c) population labeling spectra with the saturation laser tuned to the blue and red origins, respectively.

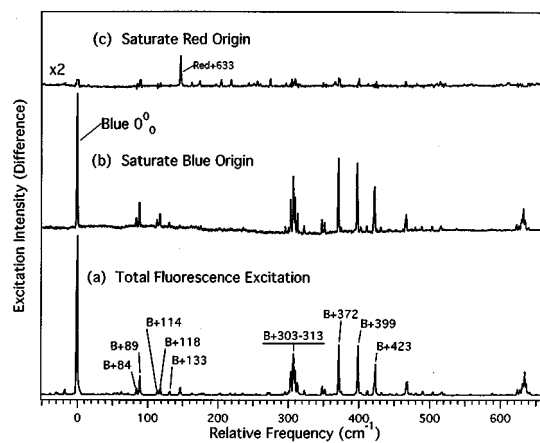


FIG. 4. (a) Fluorescence excitation spectra of the region near the blue origin in 5-hydroxytropolone. (a) Total fluorescence, (b), (c) population labeling spectra with the saturation laser tuned to the blue and red origins, respectively.

excitation spectrum of the region near the red origin (a) with population labeling spectra in which the saturation laser is tuned to the blue and red origins [(b) and (c), respectively]. Analogous spectra in the region near the blue origin are shown in Fig. 4.

A comparison of Fig. 3(a) with Figs. 3(b) and 3(c) shows that the great majority of transitions in the first  $450\text{ cm}^{-1}$  of the spectrum arise from the same ground-state level as the red origin. Similarly, nearly all the more intense transitions in the first  $600\text{ cm}^{-1}$  above the blue origin have a common ground-state level with the blue origin. Thus, the population labeling spectra cleanly partition the total fluorescence spectrum into its isomeric components. A few transitions in the fluorescence excitation spectrum do not show up in either population labeling spectrum. In most cases, these have been assigned to hot bands or clusters. Note also that, by comparison to the unsaturated excitation spectrum, the strong transitions in the population labeling spectrum are highly saturated, distorting their intensities. Imperfect signal subtraction in the population labeling spectra results in irregularities in the base line in the region of some of the strong transitions. However by aligning the normal and difference spectra, irregularities are easily distinguished from actual transitions. Note finally that the population labeling spectra highlight several surprising correlations. For example, the set of five transitions  $84\text{ to }132\text{ cm}^{-1}$  above the blue origin share a common ground state with the blue origin. Such a large number of low-frequency vibrations is quite unexpected in 5-HOTrOH, and no corresponding transitions exist in the low-frequency region above the red origin.

The dispersed emission spectra presented in the next section prove that many of the transitions in the excitation spectrum occur in pairs arising from *syn* and *anti* ground-state isomers undergoing transitions to a common excited state level. To highlight this, Fig. 5 replots the population labeling spectra of Figs. 3 and 4 with the blue origin spectrum shifted  $249\text{ cm}^{-1}$  to the red, the separation between the *syn* and *anti* ground-state zero-point levels. Excited state levels at the same energy are then aligned in the two spectra and partner

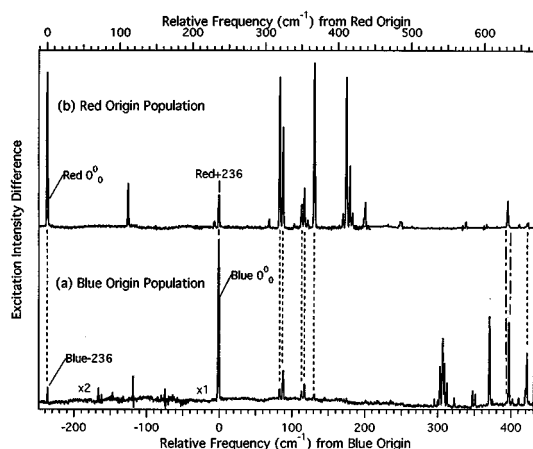


FIG. 5. Population labeling spectra of Figs. 3 and 4 replotted so that the blue spectrum is shifted  $249\text{ cm}^{-1}$  to lower frequency. The alignment of transitions in the two spectra resulting from this frequency shift are indicated by dashed vertical lines (---). These transitions have common excited state levels which originate from different isomeric ground-state zero-point levels. Also apparent in the spectra are many transitions which do not have partner transitions in the other population labeling scan. Two close-lying examples are the blue+399 and red+633  $\text{cm}^{-1}$  levels which, despite being only  $2\text{ cm}^{-1}$  separated from one another, are not partner transitions. The tie lines (- · -) show the lack of a partner transition in these bands.

transitions are connected by dashed vertical lines. Note that the transition pairs appear even in the lowest energy levels in the spectrum, i.e., including the red origin (paired with the “blue-236  $\text{cm}^{-1}$ ” transition) and blue origin (paired with the “red+236  $\text{cm}^{-1}$ ” transition). The five anomalous transitions beginning  $84\text{ cm}^{-1}$  above the blue origin also have partner transitions in the red spectrum. At the same time, some transitions do not have a partner transition from the other isomeric ground state. As we will see, the lack of a partner transition signals either (i) a poor Franck–Condon factor from one of the isomeric zero-point levels or (ii) a lack of *syn-anti* mixing in the excited state level.

The relative frequencies and intensities of the transitions in the excitation spectrum are collected in Table I as two interleaved spectra due to *anti* and *syn* ground-state populations. The tentative assignments and percent *syn/anti* character will be taken up in later sections.

## B. Dispersed fluorescence spectra of the red and blue origins

Figure 6(a) presents the dispersed fluorescence spectrum of the red  $0^0$  level following absorption at the red origin ( $25\,047\text{ cm}^{-1}$ ). Table II lists the vibronic transition frequencies (relative to the excitation frequency) and their relative intensities. We have chosen to keep tropolone’s vibrational numbering<sup>7–10</sup> in designating several of the vibrations of 5-HOTrOH which have a clear correspondence in the parent tropolone. In contrast to tropolone, the spectrum of the red  $0^0$  level of 5-HOTrOH differs by having a reduced-intensity  $26_n^0$  progression. The  $26_2^0$  transition is the only member of this progression clearly visible in the spectrum at  $-256\text{ cm}^{-1}$ , so that  $\nu_{26}'' = 128\text{ cm}^{-1}$ . This  $\nu_{26}''$  frequency is similar to its value in tropolone<sup>7</sup> ( $110\text{ cm}^{-1}$ ) and 5-aminotropolone<sup>13</sup> ( $126\text{ cm}^{-1}$ ).

TABLE I. Low-frequency vibronic transitions in the  $S_1 \leftarrow S_0$  fluorescence excitation/population labeling spectra arising from the *anti* and *syn* zero-point level populations. The frequency shifts are relative to the red origin and blue origin transitions at  $25\,047$  and  $25\,533\text{ cm}^{-1}$ , respectively.

$v' \leftarrow 0_0(\text{anti})$		$v' \leftarrow 0_0(\text{syn})$		Assignment <sup>a</sup>	<i>Syn-anti</i> mixing <sup>b</sup>
Frequency	Intensity	Frequency	Intensity		
0	100 <sup>c</sup>	(-236)	1	$a0^0$	unmixed
112	12			$a26^2$	unmixed
(236)	10	0	100 <sup>a</sup>	$s0^0$	weak
306	2				
320	79	(84)	4	$aX^1/Y^1$ Fermi	weak
325	30	(89)	12	$aW^1/X^1$ Fermi	weak
(351)	5	114	3	$s26^2/a??^d$	strong
355	8	(118)	5	$a??/s26^2^d$	strong
360	1				
369	82	(132)	2	$aY^1/Z^1$ Fermi	weak
408	1				
413	34			$aZ^1/Y^1$ Fermi	unmixed
418	7				
421	5				
438	3				
		296	2		
		301	3		
[540]		(304)	15	mostly <i>anti</i> <sup>e</sup>	strong
		307	26	mostly <i>syn</i> <sup>e</sup>	strong
		310	16	mostly <i>syn</i> <sup>e</sup>	moderate
[549]		(313)	8	mostly <i>anti</i> <sup>e</sup>	moderate
		323	3		
		348	6		
		352	4		
		372	32	$sY^1/Z^1$ Fermi	unmixed
		375	2		
633	29			$a659\text{ cm}^{-1}$	unmixed
		399	31	$sZ^1/Y^1$ Fermi	unmixed
		404	2		
648	6	412	3		
659	6	(423)	19	$aW^2$	moderate

<sup>a</sup>The excited state vibrational levels are assigned based on the predominant corresponding ground-state mode in the dispersed fluorescence spectrum from the respective level.  $a=anti$ ,  $s=syn$ .

<sup>b</sup>Unmixed (<1%), weak (1%–3%), moderate (3%–10%), strong (>10%).

<sup>c</sup>For the expansion conditions under which these measurements were made, the relative *syn* and *anti* populations gave the following intensity ratios: Red  $0_0^0$ :blue  $0_0^0$ =16:100; red  $0_0^0$ :blue-236=100:4, blue  $0_0^0$ :red+236=100:2.

<sup>d</sup>*Syn-anti* Fermi doublet.

<sup>e</sup>*Syn-anti* Fermi quartet.

The rest of the spectrum is dominated by progressions and combination bands involving three vibrations of frequency 337, 355, and  $366\text{ cm}^{-1}$ . In Table II these are designated by W, X, and Y, respectively. Franck–Condon activity in these progressions is induced either by a change in frequency or a shift in equilibrium geometry along that normal coordinate in the electronic excitation. In the harmonic approximation, overlap integrals are easily calculated as a function of two parameters related to the frequency change ( $\delta$ ) and geometry shift ( $D$ ).<sup>21</sup> Table III lists the  $\delta$  and  $D$  values along the W, X, and Y coordinates for the  $S_1 \leftrightarrow S_0$  transition determined by fitting the Franck–Condon profiles along  $W_n^0$ ,  $X_n^0$ , and  $Y_n^0$ . The comparison with *ab initio* calculations of the succeeding paper suggests that W, X, and Y are totally symmetric in-plane vibrations.

The spectrum in Fig. 6(b) is obtained by excitation of the weak transition  $236\text{ cm}^{-1}$  below the blue origin (blue -236),

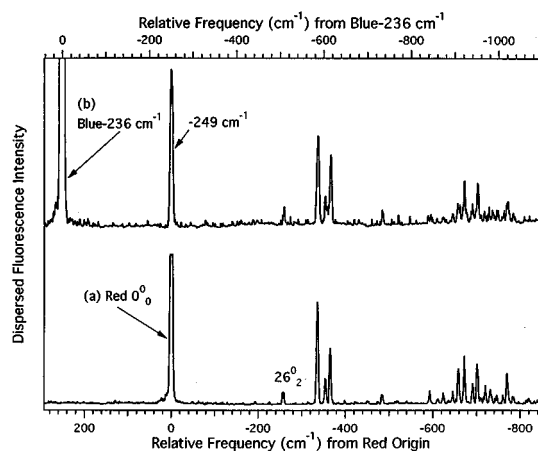


FIG. 6. Dispersed fluorescence spectra of the (a) red  $0_0^0$  and (b) blue  $-236\text{ cm}^{-1}$  transitions. The spectra are plotted on the same absolute frequency scale. The frequencies scales on the spectra are relative to the excitation frequency.

TABLE II. Low-frequency vibronic transitions from the red origin and blue origin dispersed fluorescence spectra.

Red $0^0$		Blue $0^0$	
Frequency	intensity	Frequency	intensity
0	100	0	100
193	b	249 <sup>a</sup>	15
225	2	255	16
257	9	336	63
337	50	353	33
355	19	369	83
366	37	399	18
385	1	442 <sup>a</sup>	4
400	2	506 <sup>a</sup>	2
423	b	586 <sup>a</sup>	5
453	1	591	10
483	6	604 <sup>a</sup>	7
515	2	615 <sup>a</sup>	14
592	6	625	12
623	3	657	31
646	5	671	34
659	17	689	11
673	24	706	47
691	9	723	17
701	23	735	19
709	3	739	37
720	4	745	6
732	6	772	30
747	6	781	12
762	3	890	10
772	13	921 <sup>a</sup>	15
785	5	959 <sup>a</sup>	4
820	2	980 <sup>a</sup>	5
851	3		
866	2		
893	9		
916	3		
928	3		
959	2		
981	3		

<sup>a</sup>The presence and assignment of this band is confirmed from other dispersed fluorescence spectra where it is more intense.

<sup>b</sup>From other dispersed fluorescence spectra.

TABLE III. Best-fit values for  $\delta$  and  $D$  for the W, X, Y, and Z modes of 5-hydroxytropolone.

Isomer	Normal mode (ground-state frequency, $\text{cm}^{-1}$ )	$\delta^a$	$D^b$
<i>Syn</i>	W (336)	$\sim 1.08$	
	X (353)	$\sim 1.14$	
	Y (369)	1.00	1.26
	Z (399)	1.00	0.60
<i>Anti</i>	W (337)	1.02	1.15
	X (353)	1.04	0.65
	Y (365)	1.00	0.85
	Z (400)	1.00	0.20

<sup>a</sup>The value of  $\delta$  is determined from the ground and excited state frequencies [ $\delta = (\nu''/\nu')^{1/2}$ ].

<sup>b</sup>As defined in Ref. 21.

labeled as such in Fig. 3(b). As Table I indicates, this transition is only 1% of the blue origin intensity and has the same ground state as the blue origin. The dispersed fluorescence spectra of Fig. 6 are plotted on the same absolute frequency scale, with the relative frequency scales above and below the spectra defining zero as the respective excitation frequency. Apart from the different excitation frequency, the spectra are identical, indicating that the red  $0^0$  and blue  $-236$  transitions involve excitation out of the *anti* and *syn* ground-state zero-point levels, respectively, to the same excited state level, nominally the *anti*  $0^0$  level. Thus, the red  $0^0$  level is  $236\text{ cm}^{-1}$  below the blue  $0^0$  level. Combining this with the  $485\text{ cm}^{-1}$  separation between red and blue origin transitions determines that, in the ground state the energy ordering is reversed, with the blue  $0_0$  level  $249\text{ cm}^{-1}$  below the red  $0_0$  level. Figure 1 summarizes these energy differences.

Figures 7(a) and 7(b) display the dispersed fluorescence spectra of the blue  $0^0$  level following excitation via the blue origin (a) and via the transition  $236\text{ cm}^{-1}$  above the red origin (b). The latter transition has the same ground-state level as the red origin [Fig. 3(b)]. Again, the two transitions are partners originating from the *syn* and *anti* ground-state zero-point levels, here terminating in the (nominally) *syn*  $0^0$  excited state level. The major transitions in the dispersed fluorescence spectrum of *syn*  $0^0$  (Fig. 7) are similar to, but distinct from those of the *anti*  $0^0$  level (Fig. 6). The  $26_2^0$  transition appears at  $-255\text{ cm}^{-1}$ . The dominating set of three fundamentals at 336, 353, and  $369\text{ cm}^{-1}$  are all within a few wave numbers of the corresponding W, X, and Y frequencies in the *anti* isomer, though the relative intensities within the set have changed somewhat.

The evidence presented by Figs. 6 and 7 is that the red  $+236\text{ cm}^{-1}$  and blue  $-236\text{ cm}^{-1}$  transitions are crossover transitions from *syn* ground state to a (predominantly) *anti* excited state and vice versa, as shown in Fig. 1. In keeping with this picture, the tie lines in Fig. 7(a) highlight a series of minor transitions in the blue  $0^0$  emission spectrum to transitions in the red (*anti*) well. As expected, the first such transition occurs  $+249\text{ cm}^{-1}$  from the excitation frequency, terminating in the red  $0_0$  level. The other identifiable transitions into the red well are progressions involving the vibrations at 337 (W), 355 (X), and  $366\text{ cm}^{-1}$  (Y).

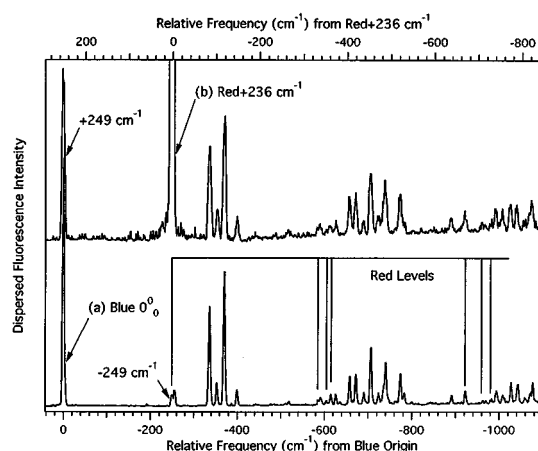


FIG. 7. Dispersed fluorescence spectra of the (a) blue  $0_0^0$  and (b) red+236  $\text{cm}^{-1}$  transitions. The spectra are plotted on the same absolute frequency scale. The frequencies scales on the spectra are relative to the excitation frequency. The tie lines in (a) highlight the transitions into the *anti* well in the ground state, at five times the sensitivity.

### C. Strategies for analyzing the *syn-anti* mixing

The excited state vibronic levels studied in the following sections possess widely varying degrees of *syn-anti* mixing. In studying the single vibronic level spectroscopy, two questions motivate our analysis. First, for each mixed level, what are the *syn* and *anti* vibrational levels contributing to the mixing? Here we seek an understanding of the vibrational mode selectivity and hope to determine if certain modes are especially important in promoting the isomerization. Second, what are the quantitative *syn* and *anti* characters for each level? The red and blue origin dispersed fluorescence spectra (Figs. 6 and 7) provide some guidance to our analysis.

(1) As shown in Fig. 1, we interpret the crossover transitions as originating from pure isomeric ground-state levels to excited state levels of mixed *syn/anti* character, i.e.,

$$\psi_{\text{grd}} = \psi_{\text{syn}} \text{ or } \psi_{\text{anti}}$$

while

$$\psi_{\text{exc}} = \alpha \psi_{\text{syn}} + \beta \psi_{\text{anti}}.$$

The deduction that it is the excited rather than the ground-state wave functions which are mixed rests on several facts. First, in tropolone the H-atom tunneling splitting is 20 times larger in  $S_1(0^0)$  than in  $S_0(0_0)$ . By analogy, in 5-HOTrOH, one would expect a much smaller barrier to H-atom tunneling in  $S_1$  than in  $S_0$ , leading to *syn-anti* mixing in the  $S_1$  state. Second, the red  $0^0$  emission spectrum [Fig. 6(a)] shows no activity in transitions to any of the blue ground-state levels which are strong in the blue  $0^0$  emission spectrum, indicating that all these blue ground-state levels are unmixed. Finally, the additivity of overtones and combination bands in the ground state does not carry over to the excited state, consistent with coupling between *syn* and *anti* levels being important in the excited state, but not the ground state.

(2) The excited state *syn-anti* mixing is not typically between *syn* and *anti* levels of the same vibrational state character. One might have expected from the presence of the

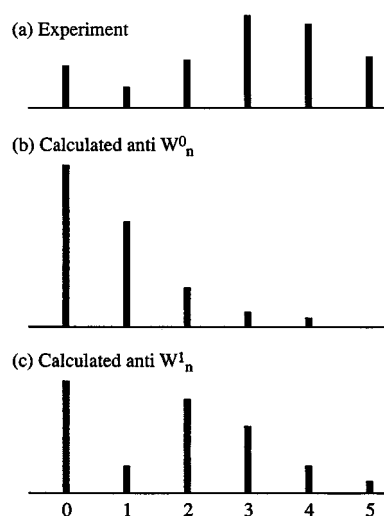


FIG. 8. (a) The experimental Franck–Condon intensity profile of the crossover transitions in emission from blue  $0^0$  to the  $W_n$  ( $337 \text{ cm}^{-1}$ ) progression in the *anti* (red) well. (b),(c) The calculated intensity profiles from  $W^0$  and  $W^1$ , respectively. The calculated values use  $\delta=1.02$  and  $D=1.15$ , the best-fit values for  $W_n^0$  from the red  $0^0$  dispersed fluorescence spectrum.

*syn*  $S_0(0_0) \leftrightarrow$  *anti*  $S_1(0^0)$  and *anti*  $S_0(0_0) \leftrightarrow$  *syn*  $S_1(0^0)$  crossover transitions that the *syn-anti* mixing experienced by the *syn* and *anti*  $0^0$  levels was a simple two-level mixing, i.e.,

$$\psi_1 = \alpha \psi_{\text{syn}}(0^0) + \beta \psi_{\text{anti}}(0^0),$$

$$\psi_2 = \beta \psi_{\text{syn}}(0^0) - \alpha \psi_{\text{anti}}(0^0).$$

However, calculations of the  $\alpha/\beta$  ratio differ by more than a factor of 3 if one uses the intensities of the red origin/blue  $-236$  and blue origin/red+236 pairs and assumes the above form for the wave functions. Furthermore, the observed “crossover” emission from blue  $0^0$  into the red well (marked by tie lines in Fig. 7) is inconsistent with emission from red  $0^0$ . As a result, the primary coupling of blue  $0^0$  is not to red  $0^0$ . Instead, the change in intensity profile of the  $337 \text{ cm}^{-1}$  progression suggests the red  $W^1$  level as the primary level coupled to blue  $0^0$ . Using the  $\delta$  and  $D$  values fitted to the  $W_n^0$  progression (Table III), Fig. 8 compares the intensities predicted along the red  $W_n^0$  and red  $W_n^1$  progressions. The better match-up with  $W^1$  is consistent with the smaller energy gap ( $\sim 80 \text{ cm}^{-1}$ ) between blue  $0^0$  and red  $W^1$  than with red  $W^0$  ( $236 \text{ cm}^{-1}$ ).

Thus, in general, one must express a given excited state vibronic level as

$$|\psi_{\text{exc}}\rangle = \alpha \left\{ \sum_i a_i |\psi_{\text{syn}}(v_i')\rangle \right\} + \beta \left\{ \sum_j b_j |\psi_{\text{anti}}(v_j')\rangle \right\}, \quad (1)$$

where  $\alpha$  and  $\beta$  give the overall *syn-anti* weightings of the excited state level while  $a_i$  and  $b_j$  determine the vibrational state character of the *syn* or *anti* levels contributing to the mixed excited state level. The coefficients  $\alpha$  and  $\beta$  are subject to normalization constraints ( $\alpha^2 + \beta^2 = 1$ ), as are the  $a_i$  and  $b_j$  ( $\sum a_i^2 = \sum b_j^2 = 1$ ).

(3) The relative intensities of a given pair of excitation transitions terminating in a common excited state level (Fig. 5) reflect not only the percent *syn/anti* character but also the Franck–Condon factors (FCFs) and relative ground-state populations of the transitions involved. For instance, if we assume that blue  $0^0$  is coupled significantly only to red ( $W^1$ ), i.e.,

$$|\psi(\text{blue } 0^0)\rangle = \alpha|0^0\rangle_{\text{syn}} + \beta|W^1\rangle_{\text{anti}} \quad (2)$$

then the intensity of the paired “red” and “blue” transitions to this excited state level will be

$$\frac{I_{\text{blue}}}{I_{\text{red}}} = \left(\frac{\alpha^2}{\beta^2}\right) \left(\frac{|\langle 0_0|0^0\rangle_{\text{syn}}|^2}{|\langle 0_0|W^1\rangle_{\text{anti}}|^2}\right) \left(\frac{N_{\text{syn}}}{N_{\text{anti}}}\right). \quad (3)$$

In cases where the FCFs for the transitions are very different, they can dominate the observed intensities, masking the percent *syn/anti* character of a given excited state level. This explains why several transitions in the excitation and population labeling spectra (Fig. 5) do not possess a partner transition out of the other conformer ground state. A notable example is the closely grouped transitions about  $300\text{ cm}^{-1}$  above the blue origin [Fig. 5(a)]. As we will see, all levels within this set possess significant red character in the emission spectrum, yet the poor FCF for the transition from the red  $0_0$  level completely suppresses the transitions from red  $0_0$  in the excitation spectrum.

(4) If a given *syn(anti)* level is coupled to more than one *anti(syn)* level, interference effects can produce unusual intensity profiles along progressions involving those levels. This can provide some insight to the nature of the levels involved in the coupling. For example, if a predominantly *anti* level is coupled to two *syn* levels  $v'_1$  and  $v'_2$ ,

$$|\psi_{\text{exc}}\rangle = \alpha(a_1|v'_1\rangle_{\text{syn}} + a_2|v'_2\rangle_{\text{syn}}) + \beta|v'_3\rangle_{\text{anti}} \quad (4)$$

the emission intensity to a given *syn* ground-state level  $v''_m$  is given by

$$\begin{aligned} I_{\text{syn}}(v''_m) &= \alpha^2 |a_1 \langle v''_m | v'_1 \rangle_{\text{syn}} + a_2 \langle v''_m | v'_2 \rangle_{\text{syn}}|^2 \\ &= \alpha^2 \{ a_1^2 |\langle v''_m | v'_1 \rangle|^2 + a_2^2 |\langle v''_m | v'_2 \rangle|^2 \\ &\quad + 2a_1 a_2 \langle v''_m | v'_1 \rangle \langle v''_m | v'_2 \rangle \}, \end{aligned} \quad (5)$$

where we have assumed that the *syn/anti* overlap integrals are negligible. The interference term in Eq. (5) is appreciable only in  $v''_m$  which have significant Franck–Condon factors from both  $v'_1$  and  $v'_2$ .

(5) Because of the dependence of the intensities in excitation on the ground-state populations of the two isomers, quantifying the percent *syn* and *anti* character of a given excited state level is best done using the dispersed emission from the level. The summed intensity of the transitions out of that level to the *syn* ( $I_{\text{syn}}^{\text{tot}}$ ) and *anti* ( $I_{\text{anti}}^{\text{tot}}$ ) ground-state wells is independent of ground-state populations. By expressing  $\psi_{\text{exc}}$  in the basis set of localized *syn* and *anti* ground-state vibrational levels, assuming negligible *syn–anti* overlap, and applying the sum rule to the *syn* and *anti* components, one can readily show that

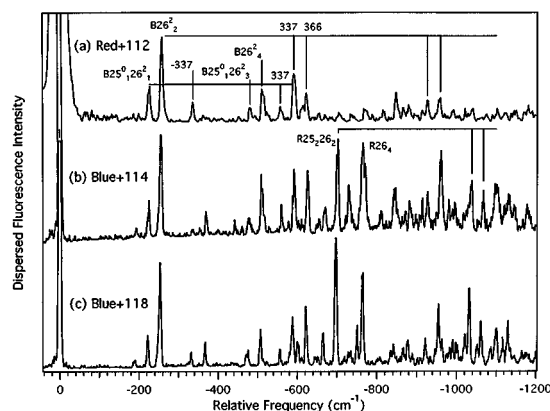


FIG. 9. Dispersed fluorescence spectra of the transitions (a)  $112\text{ cm}^{-1}$  above the red origin (red+112), (b)  $114\text{ cm}^{-1}$  above the blue origin (blue+114), and (c)  $118\text{ cm}^{-1}$  above the blue origin (blue+118). The spectra are plotted on the same absolute frequency scale. The frequency scales on the spectra are relative to the excitation frequency.

$$\frac{I_{\text{syn}}^{\text{tot}}}{I_{\text{anti}}^{\text{tot}}} = \frac{\sum_m |\langle \psi''_m | \psi_{\text{exc}} \rangle_{\text{syn}}|^2}{\sum_n |\langle \psi''_n | \psi_{\text{exc}} \rangle_{\text{anti}}|^2} = \left(\frac{\alpha''}{\beta''}\right)^2, \quad (6)$$

where  $\alpha''$  and  $\beta''$  are the *syn* and *anti* weightings of the excited state level in the localized basis set of ground-state vibrations.

Operationally, the method’s applicability is limited by the identification of transitions into the *syn* and *anti* wells, especially those terminating at higher energies where the dispersed fluorescence spectra become increasingly congested. As a result, one is often forced to cut off the sum quite low in the well where the structure is sparse enough to confidently assign transitions. This often limits integration to transitions terminating in levels in the first  $600\text{--}800\text{ cm}^{-1}$  of the *syn* and *anti* wells. Given the different vibrational state character of the mixed *syn* and *anti* excited state levels, neglecting transitions to levels higher in the wells could skew quantitative answers. As a result, the percent *syn* and *anti* characters of the excited state levels in Table I are listed by categories denoting approximate ranges of *syn* and *anti* character rather than numeric values.

## D. Dispersed fluorescence spectra from levels above the origins

### 1. Red+112

Figure 9(a) presents the dispersed fluorescence spectrum from the weak transition  $112\text{ cm}^{-1}$  above the red origin. The strong false origin at  $-257\text{ cm}^{-1}$  is due to red  $26_2$ , with increased activity in  $26_4$  as well. The great similarity of the spectrum to corresponding transitions in tropolone<sup>7–10</sup> and 5-aminotropolone<sup>13</sup> argues for assigning the red+112 transition as the red  $26_0^2$  transition.  $\nu_{26}$  is an out-of-plane vibration calculated<sup>7(c)</sup> to have out-of-phase motion of the two oxygen atoms. The major transitions built off the false origin are like those from red  $0^0$ , indicating little coupling of  $26^2$  to the vibrations involved in the main vibrational activity in the spectrum. As in 5-aminotropolone,<sup>13</sup> the weakness of this

transition and the shortness of the progression indicate that the 5-OH substitution has stiffened the planarity of the ring in the  $S_1$  state by comparison to tropolone.

The peak at  $-225\text{ cm}^{-1}$  is assigned as (red  $25_0^2 26_1^2$ ), again by analogy with 5-aminotropolone. Its presence indicates a Duschinsky effect<sup>22,23</sup> in which the normal coordinates for  $\nu_{25}$  and  $\nu_{26}$  in the ground state are mixed in the excited state.<sup>9</sup> This assignment predicts a  $97\text{ cm}^{-1}$  frequency for  $\nu_{25}''$ , compared to  $173\text{ cm}^{-1}$  in tropolone.

The red  $26^2$  level shows no evidence of coupling to blue levels in the dispersed fluorescence scan, indicating that  $\nu_{26}$  is not significantly coupled to the isomerization reaction coordinates and is nearly pure *anti* in character.

## 2. Blue+114/118 (red+350/354)

Identification of the  $26_0^2$  transition in the blue spectrum is less obvious. A comparison of frequencies suggests either blue+114 or blue+118. Both of these transitions have partners (at red+350/354) originating from the *anti* ground state, indicating that both excited state levels are of mixed *syn-anti* character. The dispersed fluorescence spectra of Figs. 9(b) and 9(c) show that the pair comprise a *syn-anti* Fermi resonance. The first  $600\text{ cm}^{-1}$  show a strong resemblance to the red+112  $\text{cm}^{-1}$  spectrum [Fig. 9(a)], indicating that blue  $26^2$  is one member of the Fermi pair. The spectra also show a strong false red origin at  $-702\text{ cm}^{-1}$  ( $-453$  relative to the red zero-point level) with red  $\nu_{26}$ , 337, and  $369\text{ cm}^{-1}$  transitions built off of it. The  $-702\text{ cm}^{-1}$  transition is flanked by a second strong red transition at  $-764\text{ cm}^{-1}$  (red  $-515\text{ cm}^{-1}$ ). The relative intensities of the red and blue transitions in the spectra of Figs. 9(b) and 9(c) reflect a somewhat greater blue  $26^2$  character in the blue+114  $\text{cm}^{-1}$  excited state level by comparison to blue+118. Thus, even though the red  $26^2$  level is virtually pure *anti*, the blue  $26^2$  level is strongly *syn-anti* mixed due to a near-degenerate *syn-anti* Fermi resonance. Given the nearly equal *syn-anti* mix of the levels, the coupling matrix element responsible for the mixing is about half the separation, i.e.,  $V_{\text{syn-anti}} \approx 2\text{ cm}^{-1}$ .

We can only suggest a tentative assignment for the red level involved in the Fermi resonance. Our assignments of  $\nu_{25}''$  and  $\nu_{26}''$  would place the red  $26_2 25_2$  level  $-453\text{ cm}^{-1}$  from the red zero-point level and  $26_4$  at  $-515\text{ cm}^{-1}$ . This suggests  $25^2 26^2$  as the red (*anti*) level in the Fermi doublet,  $\sim 354\text{ cm}^{-1}$  above the red origin with a  $\nu_{25}'$  excited state frequency of  $120\text{ cm}^{-1}$ . A difficulty with this assignment is that the red  $25_0^2 26_0^2$  transition would be expected to carry very little FC intensity, yet the red+350/354 transitions are readily observed in the fluorescence excitation spectrum.

## 3. Blue+372/blue+399

Two of the strongest transitions in the blue excitation spectrum occur 372 and  $399\text{ cm}^{-1}$  above the blue origin. Somewhat surprisingly, these transitions carry no measurable partner transitions at red+608 or red+635. Dispersed fluorescence spectra of these transitions are shown in Figs. 10(a) and 10(b). No measurable emission into the *anti* (red) well is observed, indicating that the two excited state levels accessed in these transitions are essentially pure *syn* in charac-

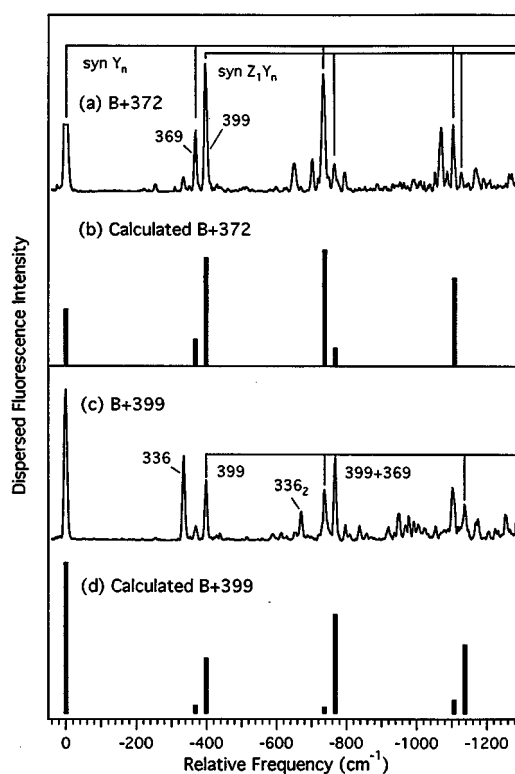


FIG. 10. Dispersed fluorescence spectra of the transitions (a) 372 and (b)  $399\text{ cm}^{-1}$  above the blue origin. The frequency scales on the spectra are relative to the excitation frequency. The peak height at the excitation frequency indicates the contribution from resonance fluorescence. (c) and (d), Stick diagrams of calculated FC profiles along  $Y_n$ ,  $Z_n$ , and  $Z_1 Y_n$  with  $a_1=0.52$ ,  $a_2=0.85$ . See the text for further details.

ter. The emission from blue+372 is dominated by a long progression in  $369\text{ cm}^{-1}$  ( $Y_n$ ) in the ground state. A strong satellite transition at  $-400\text{ cm}^{-1}$  (labeled  $Z_1$ ) terminates in a level which is quite weak in the blue origin spectrum [Fig. 7(a)].

The dispersed fluorescence spectrum from blue+399 [Fig. 10(b)] also shows considerable activity in both  $Y_n$  (with a minimum at  $n=1$ ) and  $Z_1 Y_n$ . Given the weak intensity of the transition to  $-399$  in the dispersed fluorescence from the blue origin, the strength of the blue+399 transition in excitation suggests that the transition gains its intensity through Fermi resonance coupling with a bright state. The appearance of the  $-399\text{ cm}^{-1}$  band as a strong satellite in blue+372 [Fig. 10(a)] indicates that the  $Y^1$  level ( $372\text{ cm}^{-1}$ ) is the Fermi resonant bright state.

In a simple two-state *syn-syn* Fermi resonance, the blue +372/blue+399 pair are expressed as

$$\psi(399) = a_1|Y^1\rangle + a_2|Z^1\rangle$$

and

$$\psi(372) = a_2|Y^1\rangle - a_1|Z^1\rangle.$$

The  $Z$  member of the Fermi doublet is tentatively assigned as a fundamental of a totally symmetric level since, given the small change in frequency upon electron excitation ( $\delta=1$ ), an overtone of a nontotally symmetric level (with  $D=0$  necessarily) would produce purely  $\Delta v=0$  Franck-Condon fac-

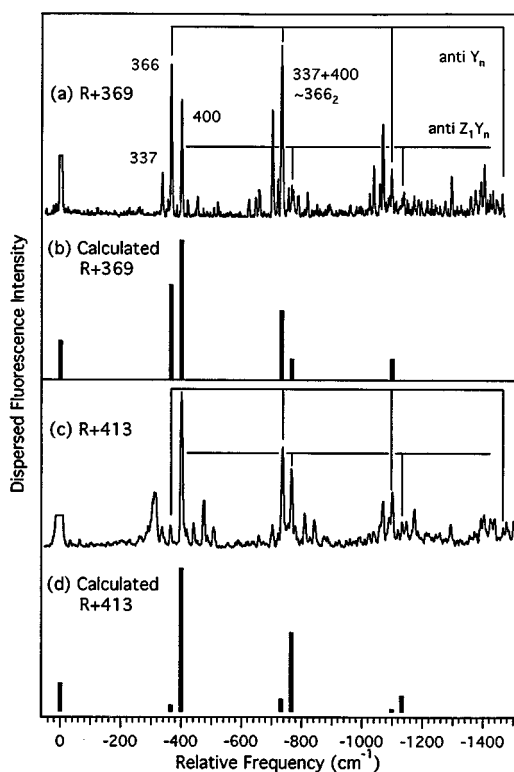


FIG. 11. Dispersed fluorescence spectra of the transitions (a) 369 and (b) 413  $\text{cm}^{-1}$  above the red origin. The frequency scales on the spectra are relative to the excitation frequency. The peak height at the excitation frequency indicates the contribution from resonance fluorescence. (c) and (d) Stick diagrams of calculated FC profiles along  $Y_n$ ,  $Z_n$ , and  $Z_1Y_n$  with  $b_1=0.43$ ,  $b_2=0.90$ . See the text for further details.

tors along  $Z$ . This is incompatible with the intensity ratio  $I(-399)/I(0_0)=0.08$  measured from the blue  $0^0$  emission spectrum [Fig. 7(a)].

Figures 10(c) and 10(d) present stick diagrams of the Franck–Condon progressions along  $Y_n$ ,  $Z_n$ , and  $Z_1Y_n$  for the best-fit coupling coefficients of  $a_1=0.52$  and  $a_2=0.85$ . Estimated errors for these coefficients are  $\pm 0.05(\pm 0.03)$  for  $a_1(a_2)$ . Overlap between certain bands (e.g.,  $2\times 369$  and  $336+399$ ) contaminates the experimental intensities of some members of the progressions. Nevertheless, the quality of the overall fit lends confidence to the assignment of blue  $+372/\text{blue}+399$  as a Fermi pair of nearly pure *syn* levels. Given the  $27 \text{ cm}^{-1}$  splitting between the levels, the matrix element coupling the levels is of order  $10 \text{ cm}^{-1}$ .

#### 4. Red+369/red+413

Figure 11 presents dispersed fluorescence spectra of the transitions 369 and  $413 \text{ cm}^{-1}$  above the red origin. The red  $+369$  transition has a very weak excitation transition partner  $133 \text{ cm}^{-1}$  above the blue origin, with an identical dispersed fluorescence spectrum. Consistent with this, the emission spectrum also exhibits weak transitions into the blue well, beginning with a transition to the *syn* zero-point level  $249 \text{ cm}^{-1}$  to the blue of the resonance peak (not shown). The crossover transitions are weak enough that no attempt was made to assess the *syn* levels involved in coupling to red  $+369$ .

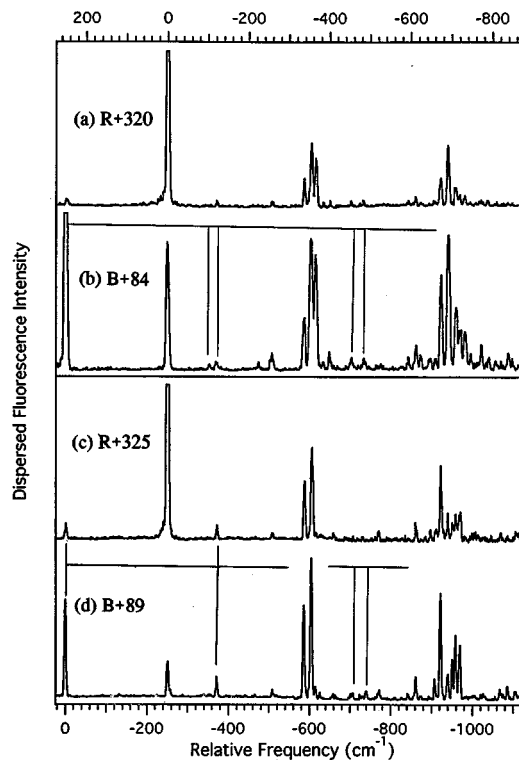


FIG. 12. Dispersed fluorescence spectra pumping the transitions (a)  $320 \text{ cm}^{-1}$  above the red origin, (b)  $84 \text{ cm}^{-1}$  above the blue origin, (c)  $325 \text{ cm}^{-1}$  above the red origin, and (d)  $89 \text{ cm}^{-1}$  above the blue origin. The most prominent transitions into the *syn* well are indicated in the figure.

The red+413 transition possesses no observable “partner” transition at blue+177. The corresponding lack of emission to *syn* levels in the ground state indicates that the excited state level is nearly pure *anti* in character.

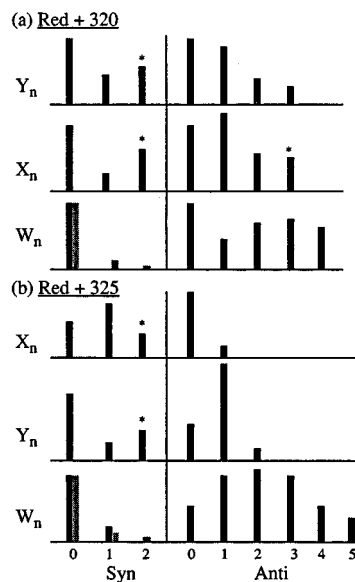


FIG. 13. Histograms of the experimental (black) and calculated (shaded) emission from (a) red+320 and (b) red+325 into the *syn* well along the  $W_n$ ,  $X_n$ , and  $Y_n$  progressions. See the text for details of the calculation.

The dispersed emission spectra of these transitions are analogous to the blue+372/blue+399 pair. An analysis similar to that used on those bands leads to their assignment as a  $Y^1/Z^1$  *anti-anti* Fermi resonance pair with

$$\psi(413) = b_1|Y^1\rangle + b_2|Z^1\rangle$$

and

$$\psi(369) = b_2|Y^1\rangle - b_1|Z^1\rangle,$$

where

$$b_1 = 0.43 \pm 0.05, \quad b_2 = 0.90 \pm 0.03.$$

Figures 11(c) and 11(d) show the simulated spectra which result from using these mixed excited states and the  $\delta$  and  $D$  values for Y and Z determined from the red origin emission spectrum. We conclude that the red+369/red+413 transitions are a Fermi resonance pair of *anti* levels experiencing only very weak coupling with levels in the *syn* well.

### 5. Red+320/325 (blue+84/89)

The dispersed fluorescence spectra of Fig. 12 are from two *syn-anti* transition pairs, the red+320/blue+84 pair and the red+325/blue+89 pair. Once again, the transitions within each pair originate from *anti/syn* ground-state zero-point levels to a common excited state level, producing identical dispersed fluorescence spectra. The stronger *syn-anti* mixing experienced by these excited state levels enables good-quality dispersed fluorescence spectra to be recorded following excitation out of either isomeric zero-point level [Figs. 12(a)–12(d)]. While the emission from both excited state levels is dominated by emission into the red (*anti*) ground-state well, both also show significant emission to the *syn* well. The most prominent of these transitions are labeled in the figure.

The two *anti* excited state levels responsible for the emission appear to be in Fermi resonance with one another. This is reflected in the significant changes (by comparison to red  $0^0$ ) along both the 337 ( $W_n$ ) and 353  $\text{cm}^{-1}$  ( $X_n$ ) progressions from either excited state level. Figure 13 presents a histogram of the relative intensities of the  $W_n$ ,  $X_n$ , and  $Y_n$  progressions into both *syn* and *anti* wells. By comparison to the red  $0^0$  dispersed fluorescence spectrum, Fig. 13 shows increased activity along *anti*  $W_n$  and  $X_n$ . This suggests the two excited state levels as an *anti*  $W^1/X^1$  Fermi resonance pair. However, quantitative fitting of the emission spectra in terms of a simple two-level  $W^1/X^1$  Fermi resonance fails to produce a satisfactory fit.

Of the possible explanations of this fact, two seem most plausible. First, the two levels may be involved in Duschinsky rotation as well as Fermi resonance. That Duschinsky rotation is present in the molecule is apparent from the  $\nu_{26}/\nu_{25}$  mixing noted earlier in the emission from  $26^2$ . Similar mixing between ground and excited state modes along W and X would produce Fermi resonance-like behavior in the emission spectra even in the absence of Fermi resonance coupling. Second, the progression intensities may be effected by the coupling of the red+320/red+325 *anti* excited state lev-

els with one or more *syn* levels. However, a proper assessment of the effects of such coupling requires a knowledge of the *syn* levels involved in the mixing.

To that end, Fig. 13 also includes histograms of the emission along  $W_n$ ,  $X_n$ , and  $Y_n$  progressions into the *syn* wells. A striking feature of this emission is the complete absence of observable activity in the *syn*  $W_n$  progression in either the red+320 or red+325 emission. Such a loss in activity can only result from destructive interference in the emission into *syn* levels. This can occur if the *anti* state is coupled with more than one *syn* level with significant Franck–Condon factors along the  $W_n$  progression (Sec. III C). Since the dispersed emission from blue  $0^0$  has already provided evidence for blue  $0^0 \leftrightarrow$  red  $W^1$  mixing, we propose additional mixing of the red  $W^1/X^1$  Fermi pair with blue  $W^1$  as the source of the destructive interference along  $W_n$ . Thus, to first order, we write  $\psi_{\text{exc}}$  as

$$\psi_{\text{exc}} = \alpha\psi_{\text{syn}} + \beta\psi_{\text{anti}},$$

where

$$\psi_{\text{syn}} = a_1|W^0\rangle_s + a_2|W^1\rangle_s$$

and

$$\psi_{\text{anti}} = b_1|W^1\rangle_a + b_2|X^1\rangle_a.$$

Using this form for the red+320 and red+325 excited state levels, the intensity of emission along  $W_n$  relative to the  $W_0$  intensity is

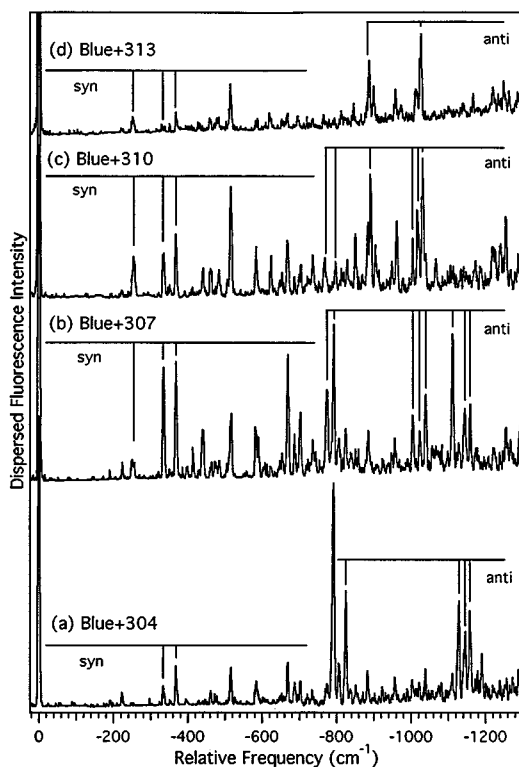


FIG. 14. Dispersed fluorescence spectra pumping the transitions (a) 303, (b) 307, (c) 310, and (d) 313  $\text{cm}^{-1}$  above the blue origin. The frequency scale is relative to the excitation frequency.

$$\frac{I(W_n)_{syn}}{I(W_0)_{syn}} = \frac{\{a_1\langle W_n|W^0\rangle_s + a_2\langle W_n|W^1\rangle_s\}^2}{\{a_1\langle W_0|W^0\rangle_s + a_2\langle W_0|W^1\rangle_s\}^2}. \quad (7)$$

The overlap integrals in Eq. (7) are readily calculated from the  $\delta$  and  $D$  values for this normal mode (Table III). The unknown coefficients are  $a_1$  and  $a_2$  which specify the fractional  $syn$   $W^0$  and  $syn$   $W^1$  character in the red+320 and red+325 levels. Figure 13 includes the calculated intensity profile along  $syn$   $W_n$  for  $a_2 \sim -a_1$ . With these values, a near-

quantitative destructive interference occurs along  $syn$   $W_n$ , consistent with what is observed experimentally. We conclude that the *anti*  $W^1$  level is coupled about equally to both  $syn$   $W^0$  and  $syn$   $W^1$ .

As suggested earlier, it is possible that this same  $syn$ –*anti* mixing is responsible for the unusual intensity profiles in the  $W_n/X_n$  emission to the *anti* ground-state well. To estimate the potential effect of coupling to  $syn$  levels on the *anti*  $W_n$  emission, one must calculate

$$\frac{I(W_{n,a})}{I(W_{0,a})} = \frac{[\alpha\{a_1\langle W_{n,a}|W_s^0\rangle + a_2\langle W_{0,a}|W_s^1\rangle\} + \beta\{b_1\langle W_{0,a}|W_a^1\rangle + b_2\langle W_{n,a}|W_a^0\rangle\langle X_{0,a}|X_a^1\rangle\}]^2}{[\alpha\{a_1\langle W_{0,a}|W_s^0\rangle + a_2\langle W_{0,a}|W_s^1\rangle\} + \beta\{b_1\langle W_{0,a}|W_a^1\rangle + b_2\langle W_{0,a}|W_a^0\rangle\langle X_{0,a}|X_a^1\rangle\}]^2}. \quad (8)$$

Our modeling of the  $W^1/X^1$  Fermi pair assumed negligible  $syn$ –*anti* overlap and thus would have neglected the  $\alpha$  terms in Eq. (8). While a unique fit is not possible without a knowledge of the  $syn$ –*anti* overlap integrals, representative calculations using reasonable values of  $\alpha$ ,  $a_1$ , and  $b_1$  show that significant effects begin to appear for  $syn$ –*anti* overlap integrals of 0.2 or larger. Hence, the unusual emission intensity profiles observed from these excited state levels which are experiencing significant  $syn$ –*anti* mixing are probably a further consequence of this mixing.

## 6. Blue+303–313

The fluorescence excitation spectrum of Fig. 4(a) shows a close-lying set of four transitions 303 to 313  $\text{cm}^{-1}$  above the blue origin. Its intensity in excitation from the  $syn$  zero-point level and its frequency relative to the blue origin suggest it as the blue analog of the red+321/325 levels, i.e., blue  $W^1/X^1$ . However, the presence of four transitions indicates some additional Fermi resonance coupling.

The dispersed fluorescence spectra of the four transitions are shown in Figs. 14(a)–14(d). All the spectra show strong  $syn$ –*anti* mixing, with significant emission into both  $syn$  and *anti* ground-state wells. The four transitions break qualitatively into two pairs (304/307 and 310/313). Within each pair, the emission spectra are similar, differing primarily in the relative intensities of the  $syn$  and *anti* emission. The blue +307 and blue+310 excited state levels have more  $syn$  character (blue emission) while the blue+304 and blue+313 peaks are more heavily weighted toward *anti*. It appears, then, that the four transitions comprise two  $syn$ –*anti* Fermi resonances, with weaker Fermi mixing within the pair of  $syn$  levels.

The blue+304/307 pair and the blue+310 transition have long progressions in  $W_n$  into the blue ( $syn$ ) well, consistent with significant  $syn$   $W^1$  character in these excited state levels. However, unlike the red+321/325 pair, no significant activity in  $X_1W_n$  [353  $\text{cm}^{-1} + n(336)$ ] is indicated.

The emission into the *anti* well is quite complicated, and we have been unable to assign the vibrational state character of the *anti* levels involved in the  $syn$ –*anti* Fermi resonances. However, partner transitions originating from the *anti* zero-

point level (which should appear at red+640–650) are not observed. Thus, the *anti* levels involved in the  $syn$ –*anti* Fermi resonance have poor Franck–Condon factors from red 0<sub>0</sub>, so that all intensity in the blue excitation spectrum derives from the  $syn$  character of the excited state levels. In this case, the intensities of the transitions in excitation can be used to determine the percent  $syn$  character of the levels, i.e.,

$$\begin{aligned} \psi(307) &= \alpha\psi_{syn} + \beta\psi_{anti}, & \psi(313) &= \gamma\psi_{syn} + \delta\psi_{anti}, \\ \psi(304) &= \beta\psi_{syn} - \alpha\psi_{anti}, & \psi(310) &= \delta\psi_{syn} - \gamma\psi_{anti}, \end{aligned}$$

leads to

$$\frac{I(307)}{I(304)} = \frac{\alpha^2}{\beta^2} = 1.73, \quad \frac{I(313)}{I(310)} = \frac{\gamma^2}{\delta^2} = 0.47.$$

We conclude that the blue+304 and blue+307 transitions are (36%  $syn$ , 64% *anti*), and (64%  $syn$ , 36% *anti*), respectively. Similarly, the blue+310 transition is 68%  $syn$ , 32% *anti*, while blue+313 is its complement.

## 7. Red+633

The red+633 transition is the strongest of the red transitions appearing above the blue origin [Fig. 14(c)]. The dispersed fluorescence spectrum from this level (not shown) exhibits a strong false origin at  $-659 \text{ cm}^{-1}$ . This transition is present in the red 0<sup>0</sup> dispersed fluorescence spectrum (Table II), and does not correspond to any overtone or combination of 25, 26, W, X, Y, or Z. We assign red+633 as a new fundamental ( $V_0^1$ ) associated with  $659 \text{ cm}^{-1}$  in the ground state. There is no evidence in the dispersed fluorescence spectrum of transitions into the  $syn$  (blue) well, nor is there an observable partner excitation transition at blue+397 (Fig. 5). This is noteworthy partly because the excited state level is only  $2 \text{ cm}^{-1}$  below blue+399, one of the strongest transitions in the blue excitation spectrum. Despite being well above the energy of many other levels experiencing strong  $syn$ –*anti* mixing, the red+633 (blue+396) and blue+399 (red+636) levels are completely decoupled from one another, with red+633 being purely *anti*, and blue+399 purely  $syn$  in character.

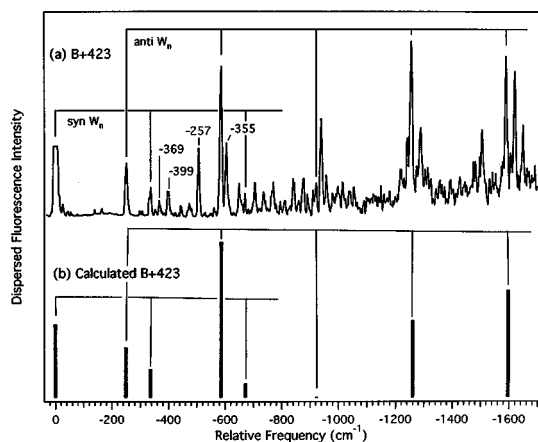


FIG. 15. (a) Dispersed fluorescence spectrum following excitation of the transition  $423\text{ cm}^{-1}$  above the blue origin ( $659\text{ cm}^{-1}$  above the red origin). (b) Histogram of the calculated emission from blue+423 into the *syn* and *anti*  $W_n$  progressions. See the text for further details of the calculation.

### 8. Blue+423/red+659

The fluorescence excitation transition  $423\text{ cm}^{-1}$  above the blue origin does not have a clear analog in the same region of the red spectrum. It does, however, exhibit a partner transition at red+659. The intensity of both blue+423 and red+659 transitions is reasonably strong (Table I), so that the excited state is a mixture of levels with good FCFs from both *syn* and *anti* ground states. Due to the larger population in the *syn* ground state, the dispersed emission spectrum of Fig. 15(a) was recorded following excitation of blue+423. However, the emission is primarily into the *anti* well, and is dominated by a long progression in  $W_n$  with a minimum at  $n=2$ . Satellite bands in  $X_1W_n$  ( $X=353\text{ cm}^{-1}$ ) analogous to those in the red 321/325 Fermi pair are also observed. The Franck–Condon profile along  $W_n$  is qualitatively accounted for as  $W_n^2$  using the  $\delta$  and  $D$  values for the progression [Fig. 15(b)], and we assign the *anti* character of the excited state level as predominantly  $W^2$ , with some Fermi mixing with  $W^1X^1$ . Of all the excited state levels studied in 5-HOTrOH, this  $W^2$  *anti* level experiences the largest *syn*–*anti* mixing of any levels which are not in near-degenerate Fermi resonance with one another. This implies that the *syn*–*anti* coupling matrix elements operating on this level are particularly large.

Emission into the *syn* levels is dominated by transitions at  $W_1(-336)$ ,  $Y_1(-369)$ , and  $Z_1(-399)$ , with  $W_n$  and  $Y_n$  progressions built on these. The activity in the pure  $W_n$  progression into the *syn* well [Fig. 15(b)] is to be contrasted with the complete lack of  $W_n$  activity in the emission from the *anti*  $W^1$  level (red+321/325). In that case (Sec. III D 4), the unusual intensity profile was accounted for as destructive interference in the emission between the *syn*  $W^0$  and *syn*  $W^1$  components of the state. If we assume a similar mixing of *anti*  $W^2$  with *syn*  $W^1$  and *syn*  $W^2$ , with mixing coefficients of equal and opposite sign, the intensity profile shown in Fig. 15(b) results. The calculated profile closely matches experiment, providing further evidence for the importance of mode  $W$  in the mixing. On the other hand, the intensity in *syn*

$Z_1(-399)$  indicates that other *syn* levels (e.g.,  $Z^1$ ) also contribute to the vibrational state mixing present in this level.

## IV. DISCUSSION AND CONCLUSIONS

The substitution of an OH group in the five position in tropolone produces a modest asymmetry in the molecule which has fascinating spectroscopic and dynamical consequences. In the ground state, the asymmetry and large isomerization barrier combine to effectively localize the molecule in either the *syn* or *anti* well, while in the  $S_1$  state, the single vibronic levels exhibit widely varying degrees of delocalization. When such delocalization occurs it is possible to excite the molecule to the mixed excited state out of either ground-state zero-point level as long as the states involved in the mixing have good Franck–Condon factors from both isomeric ground states.

### A. 5-HOTrOH as a molecular optical switch

The extreme state selectivity of the mixing enables efficient, reversible *syn*–*anti* photoisomerization of 5-HOTrOH. For instance, the red+236 crossover transition pumps the *anti* ground-state molecule to the blue  $0^0$  level, whose emission is greater than 95% into the *syn* well. Only  $15\text{ cm}^{-1}$  away is the blue–236 crossover transition, which promotes 5-HOTrOH out of the *syn* ground-state well to red  $0^0$ , whose emission is greater than 98% into the *anti* well. In contrast, the red and blue origin transitions are nearly pure *anti*↔*anti* and *syn*↔*syn* transitions, respectively. From a functional standpoint, one could categorize the blue/red origins, the blue–236, and the red+236 transitions as read, write, and erase operations of a molecular optical switch. Unlike most other schemes for optical switching, this switch is activated by individual vibronic levels within the same electronic state, rather than the electronic state-driven photoisomerization schemes typically employed.<sup>24</sup> 5-HOTrOH is also an intriguing optical switch candidate in its utilization of H-atom tunneling in the switching mechanism.

Of course, in order to be of any practical use, similar vibrational state selectivity must be achieved in the condensed phase. There is in principle much to be learned from such studies. In the condensed phase, the interactions with the surrounding matrix (whatever its composition) will likely change the relative energies of *syn* and *anti* conformers, thereby sliding the ladders of *syn* and *anti* energy levels relative to one another. This will reduce some mixings, but turn on others. Vibrational relaxation within each  $S_1$  isomeric well or between the wells could also alter the *syn*–*anti* character of the emitting state. Finally, the overlap between phonon bands for the transitions may reduce the selectivity which can be achieved except at very low temperature.

### B. Vibrational mode selectivity in the *syn*–*anti* mixing

Figure 16 presents an energy level diagram of the  $S_1$  levels of 5-HOTrOH studied in this work. The approximate *syn* and *anti* character of each of the levels is given based on the dispersed emission spectra. The overview provided by Fig. 16 highlights three categories of  $S_1$  levels.

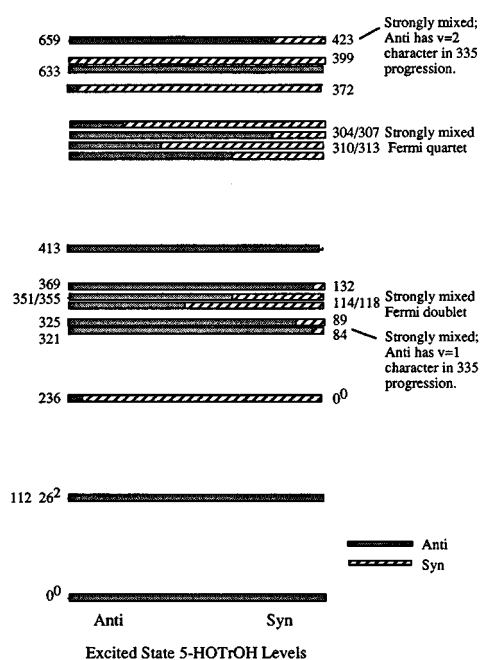


FIG. 16. Energy level diagram of prominent levels in the first 700 cm<sup>-1</sup> of the S<sub>1</sub> state of 5-HOTrOH showing the approximate percent *syn* and *anti* character of the levels.

### 1. Nearly pure *syn* or *anti* levels

Many of the levels accessed in this work are, to within our ability to measure, pure *syn* or *anti* in character. In these cases, the dispersed emission spectra show transitions only into one of the isomeric wells. At the same time, partner transitions in excitation out of the other isomeric ground state are either missing or extremely weak. Nearly pure *anti* levels include red 0<sup>0</sup>, red 26<sup>2</sup>, red+369 (red Y<sup>1</sup>/Z<sup>1</sup>), red +413 (red Z<sup>1</sup>/Y<sup>1</sup>), and red+633, while blue+372 (blue Y<sup>1</sup>/Z<sup>1</sup>) and blue+399 (blue Z<sup>1</sup>/Y<sup>1</sup>) are nearly pure *syn* levels. Note that a lack of *syn-anti* mixing does not preclude other couplings. For instance, several of these levels are involved in Fermi resonances with other vibrational levels of the same isomer (e.g., the Y<sup>1</sup>/Z<sup>1</sup> Fermi resonance).

Based on this lack of *syn-anti* mixing, the vibrational motion excited in these levels either hinders H-atom tunneling or is orthogonal to the tunneling coordinate.

### 2. Levels strongly mixed through near-degenerate *syn-anti* Fermi resonance

Some of the transitions in the excitation spectrum appear as closely spaced sets of two or more transitions. The emission spectra of these levels typically show strong emission into both *syn* and *anti* wells and bear a close resemblance to one another. The major emissions into the *syn* and *anti* wells can be identified partly by the intensity changes which occur between the spectra, reflecting the varying *syn* and *anti* characters of the excited state levels. Based on these characteristics, these excited state levels are involved in near-degenerate *syn-anti* Fermi resonances.

Examples of transitions ending in levels involved in a *syn-anti* Fermi resonance are blue+114/118 and blue+303/

307/310/313. The blue+114/118 Fermi pair has as its *syn* contributor blue 26<sup>2</sup>. By contrast, the red 26<sup>2</sup> level is a nearly pure *anti* level, suggesting that there is no inherent vibrational mode selectivity to the mixing observed at blue+114/118. Instead, the strong mixing arises from the accidental near-degeneracy with an *anti* level whose vibrational state character we have not been able to identify with certainty. Similar splittings and degrees of mixing are observed in the Fermi quadruplet at blue+303–313. In all cases, the *syn-anti* coupling matrix elements  $V_{syn-anti}$  are no more than 2 cm<sup>-1</sup>.

This category of near-degenerate *syn-anti* Fermi resonance illustrates the importance of energy resonances in tunneling. In 5-HOTrOH, the most efficient *syn-anti* mixing occurs between levels which, despite small coupling matrix elements efficiently mix due to their near-degeneracy. In the case that a single *syn* and *anti* level are involved in the coupling, the H-atom tunneling can be approximated by a single double-minimum reaction coordinate with barrier height and asymmetry specific to that pair of vibrational states.<sup>7</sup> The major effect of the energy resonance is in providing a vibrationally averaged effective potential for H-atom tunneling which is symmetric, or nearly so. Then the tunneling coordinate wave functions are to a first approximation sums and differences of the localized *syn* and *anti* wave functions, and delocalization over both wells results.

Finally, it should be noted that there are examples where even a near-degenerate *syn-anti* resonance is not sufficient to turn on *syn-anti* mixing. For example, the blue+399 (red +635) and red+633 levels have an energy separation of only 2 cm<sup>-1</sup>, yet show no evidence of coupling between them. The blue+399 level is a pure *syn* level, while the red+635 level is pure *anti*. The coupling matrix element between these two levels must be very small indeed.

### 3. Levels experiencing significant mixing over larger energy gaps: The promoter mode

Aside from the near-degenerate *syn-anti* mixing, there are several excited state levels which show significant mixing despite being comparatively isolated. In these cases, there is no obvious Fermi resonant partner state, yet emission into both *syn* and *anti* wells is readily identified in the spectrum. Examples of such transitions are the blue 0<sup>0</sup> (red +236), blue+84/89 (red+321/325), and blue+423 (red +659) transitions. The fact that these isolated levels experience significant mixing suggests that they possess unusually strong *syn-anti* coupling matrix elements which can reach across large energy gaps to produce the mixing.

The vibrational state character of these levels points out some interesting similarities between them:

- (i) The blue 0<sup>0</sup> level (*syn* W<sup>0</sup>) is coupled primarily to *anti* W<sup>1</sup>.
- (ii) Red+321/325 has primary character of an *anti* W<sup>1</sup>/X<sup>1</sup> Fermi resonance. Our analysis of the emission along the W<sub>n</sub> progression indicates a roughly equal coupling of these levels to *syn* W<sup>0</sup> and *syn* W<sup>1</sup> levels.
- (iii) The red+659 level is best described as an *anti* W<sup>2</sup> level. The analysis of emission into the *syn* well is consistent

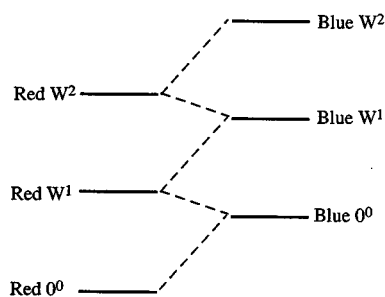


FIG. 17. A schematic energy level diagram of vibrational levels in the  $S_1$  state of 5-HOTrOH showing the major coupling routes involving the *syn* and *anti*  $W^n$  manifolds.

with roughly equal coupling of this level to both *syn*  $W^1$  and *syn*  $W^2$ , but also suggests that other *syn* levels may be involved.

These results are summarized in the energy level diagram in Fig. 17 which shows the relative energies of the *syn* and *anti*  $W^n$  progressions and the major coupling routes among these levels. Undoubtedly, the focus on the  $W^n$  character of the levels arises partly because the long progressions in  $W_n$  make the emission spectra especially sensitive to the  $W^n$  character of the levels. Nevertheless, it appears that levels that involve excitation along normal coordinate  $W$  also tend to be those with enhanced *syn-anti* mixing. Mode  $W$ , then, can be considered a promoter mode, i.e., one which is particularly strongly coupled to the *syn-anti* photoisomerization coordinate.

The coupling scheme presented in Fig. 17 bears some resemblance to schemes proposed for near-resonant vibronic coupling involving totally symmetric vibrational modes.<sup>25</sup> In that case the terms in the Hamiltonian responsible for coupling arise out of expansion of the Hamiltonian in the normal coordinates about the single global minimum in the potential energy surface. In the present case, the *syn-anti* coupling is between wave functions localized in different minima of the same electronic potential energy surface. This has the unusual consequence that adjacent levels in the same vibrational manifold (e.g., blue  $W^1$  and blue  $W^2$ ) can be indirectly coupled to one another, mediated by coupling to the same red  $W^1$  level centered on the other well.

What is the nature of the promoter mode  $W$ ? The adjoining paper takes up this question from the point of view of *ab initio* calculations on 5-HOTrOH. One candidate for mode  $W$  is the 5-HOTrOH analog of mode  $\nu_{14}$  in tropolone.<sup>10</sup> The ground and excited state frequencies of  $\nu_{14}$  are 361 and 302  $\text{cm}^{-1}$ , respectively, quite close to the 336 and 321  $\text{cm}^{-1}$  frequencies associated with  $W$ . The mode also carries good Franck-Condon activity in tropolone's spectrum, as does  $W$  in 5-HOTrOH. Finally,  $\nu_{14}$  possesses an unusually large  $S_1$

H-atom tunneling splitting of 30  $\text{cm}^{-1}$ , rivaled only by  $\nu_{13}$  (32  $\text{cm}^{-1}$ ).<sup>10</sup> Since H-atom tunneling is also responsible for *syn-anti* isomerization in 5-HOTrOH, the same vibrational modes seem likely candidates as promoter modes in the *syn-anti* isomerization.

## ACKNOWLEDGMENT

The authors gratefully acknowledge the Petroleum Research Fund, administered by the American Chemical Society, for their support of this work.

- <sup>1</sup> P. F. Barbara, P. K. Walsh, and L. E. Brus, *J. Phys. Chem.* **93**, 29 (1989).
- <sup>2</sup> Special issues devoted to excited state intramolecular proton transfer are: *Chem. Phys.* **136** (189); *J. Phys. Chem.* **95** (1991).
- <sup>3</sup> See, for example, J. A. Syage, P. M. Felker, and A. H. Zewail, *J. Chem. Phys.* **81**, 4706 (1984); T. J. Majors, U. Even, and J. Jortner, *ibid.* **81**, 2330 (1984); T. S. Zwier, E. Carrasquillo-M., and D. H. Levy, *ibid.* **78**, 5493 (1983).
- <sup>4</sup> A. Sinha, M. C. Hsiao, and F. F. Crim, *J. Chem. Phys.* **92**, 6334 (1990); A. Sinha, M. C. Hsiao, and F. F. Crim, *ibid.* **94**, 4928 (1991).
- <sup>5</sup> M. J. Bronikowski, W. R. Simpson, B. Girard, and R. N. Zare, *J. Chem. Phys.* **95**, 8649 (1991); M. J. Bronikowski, W. R. Simpson, and R. N. Zare, *J. Phys. Chem.* **97**, 2194, 2204 (1993).
- <sup>6</sup> I. Bar, Y. Cohen, D. David, T. Arusi-Parpar, S. Rosenwaks, and J. J. Valentini, *J. Chem. Phys.* **95**, 3341 (1991); R. L. VanderWal, J. L. Scott, F. F. Crim, K. Weide, and R. Schinke, *ibid.* **94**, 3548 (1991).
- <sup>7</sup> (a) R. L. Redington, Y. Chen, G. J. Scherer, and R. W. Field, *J. Chem. Phys.* **88**, 627 (1988); (b) R. L. Redington, *ibid.* **92**, 6447 (1990); (c) R. L. Redington and C. W. Bock, *J. Phys. Chem.* **95**, 10 284 (1991).
- <sup>8</sup> Y. Tomioka, M. Ito, and N. Mikami, *J. Phys. Chem.* **87**, 4401 (1983); R. Rosetti and L. E. Brus, *J. Chem. Phys.* **73**, 1546 (1980).
- <sup>9</sup> A. C. P. Alves, J. M. Hollas, H. Musa, and T. Ridley, *J. Mol. Spectrosc.* **109**, 99 (1985).
- <sup>10</sup> H. Sekiya, Y. Nagashima, and Y. Nishimura, *J. Chem. Phys.* **92**, 5761 (1990).
- <sup>11</sup> H. D. Bist, J. C. D. Brand, and D. R. Williams, *J. Mol. Spectrosc.* **21**, 76 (1966); **24**, 402 (1967).
- <sup>12</sup> J. R. Johnson, K. D. Jordan, D. F. Plasquellic, and D. W. Pratt, *J. Chem. Phys.* **93**, 2258 (1990).
- <sup>13</sup> F. A. Ensminger, J. Plassard, and T. S. Zwier, *J. Phys. Chem.* **97**, 4344 (1993).
- <sup>14</sup> F. A. Ensminger, J. Plassard, T. S. Zwier, and S. Hardinger, *J. Chem. Phys.* **99**, 8341 (1993).
- <sup>15</sup> R. Rosetti, R. Rayford, R. C. Haydon, and L. E. Brus, *J. Am. Chem. Soc.* **103**, 4303 (1981).
- <sup>16</sup> V. E. Bondybey, R. C. Haddon, and J. H. English, *J. Chem. Phys.* **80**, 5432 (1984).
- <sup>17</sup> G. D. Gillispie, M. H. Van Benthem, and M. Vangsness, *J. Phys. Chem.* **90**, 2596 (1986).
- <sup>18</sup> N. P. Ernsting, T. Arthen-Engeland, M. A. Rodriguez, and W. Thiel, *J. Chem. Phys.* **97**, 3914 (1992).
- <sup>19</sup> L. H. Spangler, R. van Zee, and T. S. Zwier, *J. Phys. Chem.* **91**, 2782 (1987).
- <sup>20</sup> G. A. Russell, C. M. Tanger, and Y. Kosugi, *J. Org. Chem.* **43**, 3278 (1978).
- <sup>21</sup>  $\delta$  is defined as  $(\nu''/\nu')^{1/2}$  and  $D$  depends on the change in geometry along the normal coordinate in going from ground to excited state. J. R. Henderson, M. Muramoto, and R. A. Willett, *J. Chem. Phys.* **41**, 580 (1964).
- <sup>22</sup> G. J. Small, *J. Chem. Phys.* **54**, 3300 (1971), and references therein.
- <sup>23</sup> E. R. Davidson, H. J. Elston, and C. S. Parmenter, *Chem. Phys. Lett.* **197**, 123 (1992).
- <sup>24</sup> C. A. Mirkin and M. A. Ratner, *Annu. Rev. Phys. Chem.* **43**, 719 (1992).
- <sup>25</sup> G. Fischer and R. Naaman, *Chem. Phys.* **12**, 367 (1976).